2002

Modeling the Effects of Electrode Composition and Pore Structure on the Performance of Electrochemical Capacitors

Changqing Lin
University of South Carolina - Columbia

Branko N. Popov
University of South Carolina - Columbia, popov@engr.sc.edu

Harry J. Ploehn
University of South Carolina - Columbia, ploehn@cec.sc.edu

Publication Info

Journal of the Electrochemical Society, 2002, pages A167-A175.

Publisher's link: http://dx.doi.org/10.1149/1.1431575
DOI: 10.1149/1.1431575

Journal of The Electrochemical Society, **149** (2) A167-A175 (2002)
0013-4651/2002/149(2)/A167/9/$7.00 © The Electrochemical Society, Inc.

Modeling the Effects of Electrode Composition and Pore Structure on the Performance of Electrochemical Capacitors

Changqing Lin, Branko N. Popov,* and Harry J. Ploehn[z]

Department of Chemical Engineering, University of South Carolina, Swearingen Engineering Center, Columbia, South Carolina 29208, USA

This work presents a mathematical model for charge/discharge of electrochemical capacitors that explicitly accounts for particle-packing effects in a composite electrochemical capacitor consisting of hydrous RuO_2 nanoparticles dispersed within porous activated carbon. The model is also used to investigate the effect of nonuniform distributions of salt in the electrolyte phase of the electrode in the context of dilute solution theory. We use the model to compare the performance of capacitors with electrodes made from different activated carbons and to investigate the effects of varying carbon content and discharge current density. Even at low discharge current density, concentration polarization in the electrodes results in underutilization of the electrodes' charge-storage capability, and thus decreased performance. Among various types of activated carbons, those with large micropore surface areas and low meso- and macropore surface areas are preferred because they give high double-layer capacitance and favor efficient packing of RuO_2 nanoparticles, thus maximizing faradaic pseudocapacitance. Increasing the electrode carbon content decreases the delivered charge and energy density, but the reductions are not severe at moderate carbon content and high discharge current. This suggests the possibility of optimizing the carbon content to minimize cost while achieving acceptable discharge performance.
 [DOI: 10.1149/1.1431575]

Manuscript submitted April 9, 2001; revised manuscript received September 24, 2001. Available electronically January 7, 2002.

Electrochemical capacitors are urgently needed as components in many advanced power systems requiring high power density, high energy density, and high cycleability.[1-6] Energy storage mechanisms in an electrochemical capacitor include separation of charge at the interface between a solid electrode and a liquid electrolyte, leading to double-layer (DL) capacitance, and faradaic redox reactions occurring at or near a solid electrode surface, known as pseudocapacitance. Charge storage in DL capacitance is essentially electrostatic in nature, and so DL charge/discharge processes are usually highly reversible. Pseudocapacitance, originating from faradaic redox reactions of oxides like RuO_2, IrO_2, or Co_3O_4 at or near the electrode surface, involves interfacial reaction as well as mass transfer of ionic charge across the double layer.[6]

Capacitors employing both DL and pseudocapacitance generally perform better than those featuring just one kind of capacitance. Activated carbon has been frequently used because its porous structure and large internal surface area result in electrodes with high specific energy and specific power densities.[6] The pore structure of activated carbon is a significant element in determining electrochemical capacitor performance. Shi[7] argued that pores of different sizes (micro-, meso-, and macropores) play different roles in contributing to DL capacitance. Macropores make a small contribution to the total specific surface area and thus contribute little to the DL capacitance. At the other extreme, micropores are responsible for most of the specific surface area, but the smallest pores may not be accessible to the electrolyte and thus do not contribute to the DL capacitance. Nevertheless, Shi claims that much of the charge storage occurs in pores with diameters less than 2 nm.

The hydrous form of ruthenium oxide ($RuO_2 \cdot xH_2O$) has been identified as an excellent electrode material for electrochemical capacitors.[8,9] Its redox reaction (shown later) produces significant pseudocapacitance as well as some contribution to DL capacitance. However, the low porosity of the native material leads to a sharp decrease in power density at high charge/discharge rates. Low power density combined with its high cost make pure $RuO_2 \cdot xH_2O$ unsuitable for commercial electrochemical capacitor applications. To improve power density, high rate performance, and cost, recent electrochemical capacitor research has focused on developing nanostructured $RuO_2 \cdot xH_2O$-carbon composite materials.[1-3] These materials have a high DL capacitance originating from high surface area of porous activated carbon, plus pseudocapacitance derived from the redox reactions of RuO_2 dispersed over the carbon surface. Dispersing the RuO_2 as nanoparticles improves the utilization of the redox active material. Thus the RuO_2 nanoparticle size and the efficiency of its dispersion on the carbon surface are variables that may affect electrochemical capacitor performance.

Various mathematical models have been developed to investigate the relationship between performance and material characteristics in the electrochemical capacitors. Johnson and Newman[10] developed a model to describe DL charging in an electrochemical cell and to predict the specific energy and power densities of electrochemical capacitors.[11] Srinivasan and Weidner[12] presented an electrochemical capacitor model that assumed a uniform salt concentration profile and faradaic processes with features similar to those of capacitors. With these assumptions, their model yielded analytical solutions for discharge performance. Lin *et al.*[13] developed a model to account for both DL capacitance and faradaic redox reactions in an electrochemical capacitor. Other simplified models in the literature have been reviewed previously.[12,13]

All previous models have assumed a single value of electrode porosity and a uniform diameter for dispersed oxide particles. No previous models have considered the effect of varying pore structure, electrode composition (*e.g.*, loading of RuO_2 in carbon), or size distribution of dispersed oxide particles on electrochemical capacitor performance. Related modeling work has considered the effects of the particle size distribution (PSD) and electrode composition for porous intercalation electrodes. Nagarajan *et al.*[14] developed a model to study the effects of PSD on the galvanostatic discharge behavior of the lithium/separator/intercalation electrode system. Packing theory was used to calculate the specific surface area and porosity of electrodes composed of materials having two characteristic particle sizes. The model was used to investigate capacity and utilization effects on the galvanostatic charge/discharge of electrodes composed of binary mixtures of spherical particles. Darling and Newman[15] also modeled a porous intercalation electrode with two characteristic particle sizes and found that PSD had an even more pronounced influence on the open-circuit behavior. Heikonen *et al.*[16] considered the effects of PSD on the discharge behavior of a nickel-metal hydride cell. Card *et al.*[17] developed a model for an activated-carbon, packed-bed electrochemical reactor that considered the effects of both micropores and macropores.

In this paper, we extend our previous model[13] by using packing theory[14] to account for varying composition and particle size effects on electrochemical capacitor performance. The model is also used to investigate the salt concentration distribution in the electrolyte phase, although we are limited by the use of dilute solution theory.

* Electrochemical Society Active Member.
[z] E-mail: ploehn@engr.sc.edu

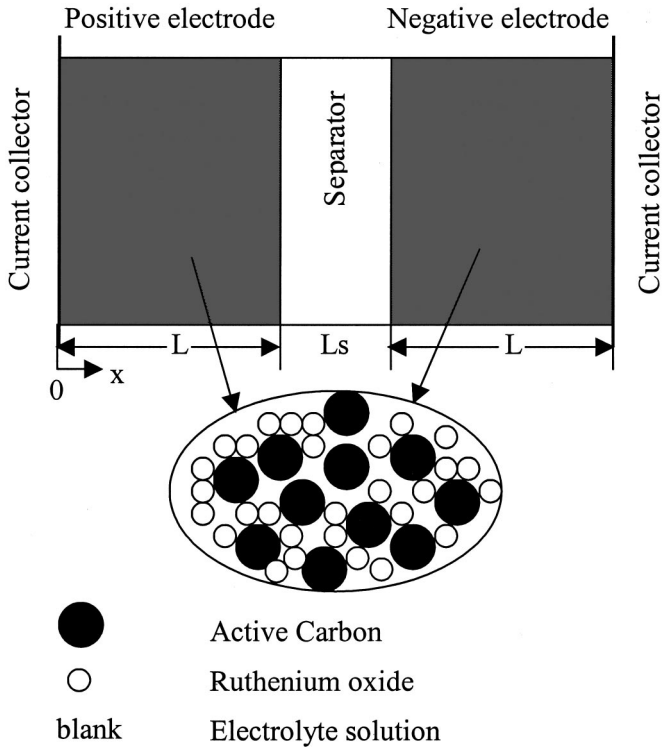

Figure 1. Schematic diagram of an electrochemical capacitor, including the model's representation of the effective structure within the porous electrode.

The model can be used to optimize the electrode composition to lower costs and improve the electrochemical capacitor's energy density, power density, and high rate performance.

Model Description

Assumptions.—The model presented here represents an extension of the general model of porous electrodes developed by Newman and Tiedemann.[18,19] Here, we consider an electrochemical capacitor (shown schematically in Fig. 1) featuring composite porous electrodes using active carbon as the support for dispersed RuO_2 nanoparticles. The electrolyte is 3.0 M H_2SO_4. The model assumes that the faradaic redox reactions[13] occur within the positive and negative electrodes given by

$$H_{0.8}RuO_2 \cdot xH_2O \underset{\text{Discharge}}{\overset{\text{Charge}}{\rightleftarrows}} H_{0.8-\delta}RuO_2 \cdot xH_2O + \delta H^+ + \delta e^- \quad [1]$$

and

$$H_{0.8}RuO_2 \cdot xH_2O + \delta H^+ + \delta e^- \underset{\text{Discharge}}{\overset{\text{Charge}}{\rightleftarrows}} H_{0.8+\delta}RuO_2 \cdot xH_2O \quad [2]$$

The model neglects any other side reactions as well as the effects of temperature variations. Furthermore, the model assumes that the DL capacitance is independent of applied potential. With respect to the electrolyte phase, transport phenomena are assumed to be governed by dilute solution theory[18] involving binary electrolyte with a single-phase solvent. Diffusion coefficients are assumed to be independent of salt concentration. The solvent velocity serves as the reference velocity when determining values for transport properties like transference numbers and diffusion coefficients.

Governing equations.—The current density passing from the solid to the electrolyte phase varies with position in each electrode according to[13]

$$\frac{\partial i_2}{\partial x} = S_d C_d \frac{\partial(\Phi_1 - \Phi_2)}{\partial t} + S_f j_f \quad [3]$$

where i_2 is the superficial current density in the electrolyte phase. The first term on the right represents DL charge/discharge, and the second term represents charge production by the faradaic redox reactions, Eq. 1 and 2. Equation 3 differs from that used in previous work[13] in that the specific surface area for DL charge/discharge, S_d, is not the same as the specific surface area for the faradaic redox reactions, S_f. One of the main objectives here is to develop expressions for S_d, S_f, and electrode porosity ϵ based on the specified composition of the electrode, the carbon pore size distribution, and the known RuO_2 particle size.

The composite electrode consists of large, irregular particles of porous carbon-containing dispersed RuO_2 nanoparticles. Shi, in his tabulation of the structural properties of many commercial activated carbons,[7] divided the carbon specific surface area into internal and external contributions based on the pore size distribution. Only micropores (pore width less than 2 nm) contribute to the internal surface area ($\hat{S}_{C,int}$). Meso- and macropores (pore width greater than 2 nm) are responsible for external surface area ($\hat{S}_{C,ext}$). RuO_2 particles of uniform diameter d_{Ru} are generally too large to fit inside micropores, but they do pack within the carbon's meso- and macropores. To account for the effect of RuO_2 particle packing on porosity, we define an effective spherical particle diameter for the activated carbon, d_C, defined by

$$d_C = \frac{6}{\hat{S}_{C,ext}\rho_C} \quad [4]$$

based on the external surface area of the carbon that is accessible to the RuO_2 nanoparticles. The RuO_2 nanoparticles pack into the pores of the carbon as shown schematically in Fig. 1. Packing theory (detailed in the Appendix) provides the value of ϵ as a function of d_C, d_{Ru}, and the composition of the electrode.

Once ε has been determined, S_d and S_f may be expressed in terms of $\hat{S}_{C,int}$, $\hat{S}_{C,ext}$, and d_{Ru}. We assume that all of the surface contributes to DL capacitance. Thus

$$S_d = (\hat{S}_{C,int} + \hat{S}_{C,ext})\rho_C x_C(1 - \varepsilon) + \frac{6x_{Ru}(1 - \varepsilon)}{d_{Ru}} \quad [5]$$

However, only the RuO_2 surface is redox-active and contributes to the pseudocapacitance, so

$$S_f = \frac{6x_{Ru}(1 - \varepsilon)}{d_{Ru}} \quad [6]$$

The volume fractions may be expressed in terms of mass fractions as shown in the Appendix.

The other governing equations are similar to those given previously.[13] The conservation of charge and Ohm's law in the matrix phase lead to

$$\frac{\partial i_1}{\partial x} + \frac{\partial i_2}{\partial x} = 0 \quad [7]$$

$$i_1 = -\sigma \frac{\partial \Phi_1}{\partial x} \quad [8]$$

Concentration polarization in the electrolyte, not considered previously, is considered here. In the context of concentrated solution theory,[18] a mass balance on salt leads to

$$\varepsilon \frac{\partial C_s}{\partial t} = \frac{\partial}{\partial x}\left[\varepsilon D_s\left(1 - \frac{d(\ln C_0)}{d(\ln C_s)}\right)\frac{\partial C_s}{\partial x}\right] + \left[\frac{S_d C_d}{2F}\frac{\partial(\Phi_1 - \Phi_2)}{\partial t} + \frac{S_f j_f}{2F}\right](1 - t_+^0) - \frac{i_2}{z_+ \nu_+ F}\frac{\partial t_+^0}{\partial x} \quad [9]$$

The second term on the right accounts for the source/sink of ions due to electrode reactions as well as DL charging and discharging.

The current distribution in the electrolyte phase is

$$i_2 = -\kappa_p \frac{\partial \Phi_2}{\partial x} - \frac{\kappa_p RT}{F}\left(1 + \frac{\partial(\ln f_\pm)}{\partial(\ln C_s)}\right)\left(\frac{s_+}{n\nu_+} + \frac{t_+^0}{z_+\nu_+}\right)\frac{\partial(\ln C_s)}{\partial x} \quad [10]$$

Equation 9 and 10 can account for variations of transference number and activity coefficient with salt concentration if appropriate activity coefficient data are available. Here, we ignore these corrections and work under the assumptions of dilute solution theory.[18]

The molar fraction of oxidized species, θ, can be related to faradaic transfer current, j_f, by[13]

$$\frac{\partial \theta}{\partial t} = \frac{S_f j_f}{Q_{f,ox} - Q_{f,re}} \quad [11]$$

where $Q_{f,ox}$ and $Q_{f,re}$ are the faradaic charge (per unit volume) of fully oxidized and reduced electrodes, respectively. If we assume Butler-Volmer kinetics for electrode reactions, we have

$$j_f = i_0\{\exp[\alpha_a(\Phi_1 - \Phi_2 - U_1)F/RT] - \exp[-\alpha_c(\Phi_1 - \Phi_2 - U_1)F/RT]\} \quad [12]$$

where U_1 is the equilibrium potential for the electrode reaction. Previous studies[9,13] have assumed empirical expressions relating U_1 to θ for the redox reactions of RuO_2, namely

$$U_1 = V_0(1 + \theta) \quad [13]$$

$$U_1 = V_0(1 - \theta) \quad [14]$$

at the positive and negative electrodes, respectively, where V_0 is initial equilibrium potential before charging, taken as 0.5 V. We follow previous studies in this regard by not accounting for the explicit dependence of kinetic expressions on local electrolyte concentration.

Defining the local potential as $E = \Phi_1 - \Phi_2$ and assuming transference numbers and activity coefficients that are independent of salt concentration, Eq. 3 and 7-10 can be combined to yield

$$S_d C_d\left(\frac{1}{\sigma} + \frac{1}{\kappa_p}\right)\frac{\partial E}{\partial t} = \frac{\partial^2 E}{\partial x^2} - \frac{RT}{F}\left(\frac{s_+}{n\nu_+} + \frac{t_+^0}{z_+\nu_+}\right)\frac{\partial^2(\ln C_s)}{\partial x^2} - S_f\left(\frac{1}{\sigma} + \frac{1}{\kappa_p}\right)j_f \quad [15]$$

$$\frac{\partial C_s}{\partial t} = D_s\frac{\partial^2 C_s}{\partial x^2} + \frac{S_d C_d(1 - t_+^0)}{2\varepsilon F}\frac{\partial E}{\partial t} + \frac{S_f(1 - t_+^0)}{2\varepsilon F}j_f \quad [16]$$

Boundary conditions include[13]

$$\text{At } x = 0,\ t > 0: \quad \frac{\partial E}{\partial x} = -\frac{I_{cell}}{\sigma} \quad [17]$$

$$\frac{\partial C_s}{\partial x} = 0$$

$$\text{At } x = L,\ t > 0: \quad \frac{\partial E}{\partial x} = -\frac{I_{cell}}{\kappa_p} \quad [18]$$

$$-\frac{I_{cell}}{F} = N_+ - N_- \approx N_+ = -2\varepsilon_s D_{s,s}\frac{\partial C_s}{\partial x} - \frac{I_{cell} t_+^0}{F}$$

In the above equation, ε_s is the separator porosity and $D_{s,s}$ is the salt diffusion coefficient in the pore of the separator. Equation 18 assumes that the concentration gradient, flux, and potential are continuous at the electrode-separator interface. Unlike the electrode phase, the effects of DL charging/discharging are neglected in the separator. Finally, Eq. 18 recognizes that the electrolyte phase carries all cell current at the electrode-separator interface, and that the anion flux is negligible compared to the cation flux there.

Initial conditions for discharge are

$$\text{At } t = 0: \quad E = 2V_0 \equiv E_0 \quad \theta = 1 \quad C_s = C_{s0} \quad [19]$$

Equation 11, 12, 15, and 16 can be solved together with these boundary and initial conditions.

Dimensional analysis.—First, we cast the equations in dimensionless form by defining the following dimensionless variables

$$\mathrm{E} = \frac{E}{E_0}, \quad C = \frac{C_s}{C_{s0}}, \quad J = \frac{j_f}{i_0}, \quad U = \frac{U_1}{E_0}$$

$$X = \frac{x}{L}, \quad \tau = \frac{t}{t_0} \quad [20]$$

where

$$t_0 = \frac{S_d C_d L^2}{\kappa_p}\left(1 + \frac{\kappa_p}{\sigma}\right) \quad [21]$$

and $E_0 \equiv 2V_0$ was defined for convenience in Eq. 19. Thus, the time scale of the problem is scaled by a characteristic time for discharge of the DL. The system of equations has the dimensionless form

$$\frac{\partial \mathrm{E}}{\partial \tau} = \frac{\partial^2 \mathrm{E}}{\partial X^2} - \frac{RT}{FE_0}\left(\frac{s_+}{n\nu_+} + \frac{t_+^0}{z_+\nu_+}\right)\frac{\partial^2(\ln C)}{\partial X^2} - \frac{S_f i_0}{E_0 S_d C_d/t_0}J \quad [22]$$

$$\frac{\partial \theta}{\partial \tau} = \frac{S_f i_0 t_0}{Q_{f,ox} - Q_{f,re}}J \quad [23]$$

$$\frac{\partial C}{\partial \tau} = \frac{D_s t_0}{L^2}\frac{\partial^2 C}{\partial X^2} + \frac{(1 - t_+^0)S_f t_0 i_0}{2\varepsilon F C_{s0}}J + \frac{S_d C_d(1 - t_+^0)E_0}{2\varepsilon F C_{s0}}\frac{\partial \mathrm{E}}{\partial \tau} \quad [24]$$

$$J = \exp\left[\frac{E_0 F}{RT}\alpha_a(\mathrm{E} - U)\right] - \exp\left[-\frac{E_0 F}{RT}\alpha_c(\mathrm{E} - U)\right] \quad [25]$$

with the following boundary and initial conditions

$$\text{At } X = 0,\ \tau > 0: \quad \frac{\partial \mathrm{E}}{\partial X} = -\frac{I_{cell} L}{E_0 \sigma} \quad \frac{\partial C}{\partial X} = 0 \quad [26]$$

$$\text{At } X = 1,\ \tau > 0: \quad \frac{\partial \mathrm{E}}{\partial X} = -\frac{I_{cell} L}{E_0 \kappa_p} \quad \frac{\partial C}{\partial X} = \frac{(1 - t_+^0)I_{cell} L}{2\varepsilon_s D_{s,s} C_{s0} F} \quad [27]$$

$$\text{At } \tau = 0: \ \mathrm{E} = 1,\ C = 1,\ \theta = 1 \quad [28]$$

Table I. Model parameters.

Parameter	Value	Reference
D_{+0}	9.312×10^{-5} cm^2/s	Newman[20]
D_{-0}	1.065×10^{-5} cm^2/s	Newman[20]
ε_s	0.7	Pillay and Newman[24]
t_+^0	0.814	Calculated from D_{+0} and D_{-0}
i_0	10^{-5} A/cm^2	Assumed
α_a	0.5	Assumed
α_c	0.5	Assumed
d_{Ru}	5 nm	Assumed
C_d	2×10^{-5} F/cm^2	Assumed
L	5×10^{-3} cm	Assumed
L_s	2.5×10^{-3} cm	Assumed
σ	10^5 S/cm	Trasalti and Lodi[23]
ρ_C	1.80 g/cm^3	Assumed
ρ_{Ru}	2.50 g/cm^3	Zheng *et al.*[8]
T	298 K	Assumed

The solution of these equations provides the distributions of local potential difference and salt concentration in the electrode. The total dimensionless potential drop across the capacitor can be expressed as

$$\bar{\Phi}_{cell} = (\bar{\Phi}_1)_+ - (\bar{\Phi}_1)_- \quad [29]$$

where $(\bar{\Phi}_1)_+$ and $(\bar{\Phi}_1)_-$ denote the dimensionless potentials ($\bar{\Phi}_1 = \Phi_1/E_0$) at the current collectors of the positive and negative electrodes, respectively. Equation 29 can be written as

$$\bar{\Phi}_{cell} = 2[\mathrm{E}|_{X=0} - V_0] - 2[\bar{\Phi}_2|_{X=1} - \bar{\Phi}_2|_{X=0}] - \frac{I_{cell}L_s}{E_0\kappa_s} \quad [30]$$

in which the three terms represent the potential differences between the solid and the electrolyte, across the electrolyte phase within the electrodes, and across the separator. The third term assumes that Ohm's law applies in the separator and ignores concentration polarization there. The second and third terms cannot be neglected if the discharge current density is high, because concentration polarization makes a significant contribution to cell potential in such cases.

The dimensionless potential in the electrolyte phase, $\bar{\Phi}_2 = \Phi_2/E_0$, may be determined after solving Eq. 22-25. The necessary governing equation, derived from Eq. 7, 8, and 10, is

$$\frac{\partial^2 \mathrm{E}}{\partial X^2} + \left(1 + \frac{\kappa_p}{\sigma}\right)\frac{\partial^2 \bar{\Phi}_2}{\partial X^2} + \frac{\kappa_p}{\sigma}\frac{RT}{FE_0}\left(\frac{s_+}{n\nu_+} + \frac{t_+^0}{z_+\nu_+}\right)\frac{\partial^2(\ln C)}{\partial X^2} = 0 \quad [31]$$

with the boundary conditions

$$\text{At } X = 0,\ \tau > 0,\ \bar{\Phi}_2 = 0 \quad [32]$$

$$\text{At } X = 1,\ \tau > 0,\ \frac{\partial \bar{\Phi}_2}{\partial X} = \frac{I_{cell}L}{E_0\kappa_p} \quad [33]$$

Equations 22-25 and 31 can be solved numerically using the DASPK solver.[20]

Model parameters.—Table I shows the base set of system parameters. The effective diffusion coefficients and ionic conductivity within the porous electrode are porosity-dependent functions given by[18,21]

$$D_i = D_{i0}\varepsilon^{0.5} \quad (i = +, -, s) \quad [34]$$

$$D_{s,s} = D_{s0}\varepsilon_s^{0.5} \quad [34a]$$

and

$$\kappa_p = \kappa_{p0}\varepsilon^{1.5} \quad [35]$$

where the subscript 0 denotes bulk solution values. Ionic conductivity in the bulk solution, κ_{p0}, can be calculated from the ion diffusion coefficients by

$$\kappa_{p0} = F^2\sum_i \frac{z_i^2 D_{i0} C_i}{RT} \quad (i = +, -) \quad [36]$$

in the context of dilute solution theory. The salt diffusion coefficient is defined by

$$D_{s0} = \frac{D_{+0}D_{-0}(z_+ - z_-)}{z_+D_{+0} - z_-D_{-0}} \quad [37]$$

The faradaic charge of a fully reduced electrode, $Q_{f,re}$, is set to zero, while $Q_{f,ox}$ can be estimated as[13]

$$Q_{f,ox} = \frac{S_f \delta F}{h^2 L_A} \quad [38]$$

where $\delta = 0.5$ for a fully charged electrode, and h is approximately 0.4 nm.

Relative available charge.—Galvanostatic discharge curves are of key interest. Dimensionless cell potential is plotted as a function of relative available charge (RAC), defined as

$$\mathrm{RAC} = \frac{I_{cell} \cdot t}{C_{total}} \quad [39]$$

where C_{total} is the total available charge in a pure RuO_2 electrode (per unit electrode area). This represents a theoretical maximum charge that could be stored in a capacitor based on RuO_2. Assuming that pure RuO_2 manifests both faradaic and DL capacitance, and that C_d for RuO_2 is the same as that for carbon, C_{total} can be estimated as

$$C_{total} = L[Q_{f,ox} + C_d S_d(E_0 - V_0)]_{x_{Ru}=1.0} \quad [40]$$

where $E_0 \equiv 2V_0$ is the initial local potential difference between the matrix and electrolyte phases. Zheng *et al.*[8] have suggested that the actual value of C_d for RuO_2 may be less than that of carbon. A more realistic value for C_d would simply shift the scale for RAC. Not only does RAC serve as a dimensionless time, but it also indicates the total available charge in a composite capacitor relative to one having pure RuO_2 electrodes, thus providing an absolute scale for RuO_2 utilization.

Results and Discussion

Effect of concentration polarization.—The present model builds upon previous work[12,13] by considering the effects of concentration polarization in the electrolyte phase. One might ask whether the improvement in the model's physical realism justifies the additional computational burden (Eq. 9, etc.). Figure 2 addresses this issue by comparing theoretical discharge curves for pure RuO_2 electrodes computed with and without concentration polarization. As shown in Fig. 2, including concentration polarization in the model leads to a decrease of about 25% in the predicted value of RAC at the end of discharge, even for a relatively low current density. With increasing current density or decreasing porosity, the effects of concentration polarization should become even more significant. These effects are now considered in more detail.

Effect of activated carbon type.—Data tabulated by Shi[7] show that the external surface areas of activated carbons vary widely. In

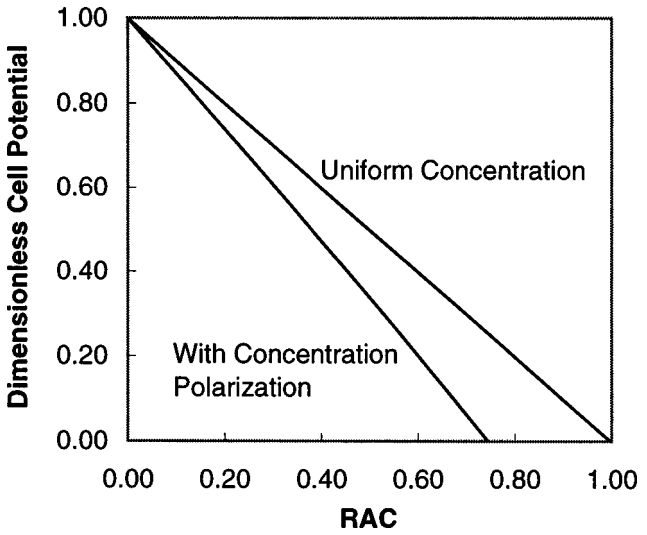

Figure 2. Effect of concentration polarization on the galvanostatic discharge of an electrochemical capacitor composed of pure RuO_2 ($x_C = 0$). Other parameters include $\varepsilon = 0.375$, $I_{cell} = 0.01$ A/cm^2, and $C_{s0} = 3.0$ M.

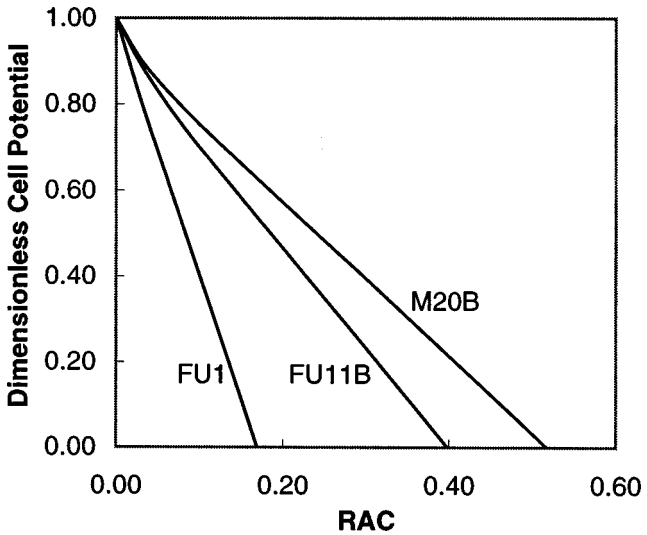

Figure 3. Galvanostatic discharge curves for capacitors employing various types of activated carbons. Parameters include $I_{cell} = 1.0$ A/cm^2, $C_{s0} = 3.0$ M, and $x_C = 0.75$.

the context of the present model, this implies that the equivalent carbon particle size, electrode porosity, and surface area for double-layer capacitance also varies widely for different carbons. The model presented here can be used to compare the performance of various carbons in electrochemical capacitors. Parameters for three selected carbons are shown in Table II. For now, the mass fractions of RuO_2 and carbon are fixed at 0.32 and 0.68, respectively, leading to a carbon volume fraction of about 0.75. This value has been found previously[14] to maximize the specific surface area and minimize electrode porosity.

Figure 3 presents the galvanostatic discharge curves for capacitors with composite electrodes made from various activated carbons. The discharge starts at a cell potential of 1.0 V, below the potential where hydrogen evolution starts, and ends at 0.0 V (both made dimensionless by $2V_0 = 1.0$ V). The area under the discharge curve is proportional to amount of charge actually delivered. The RAC value at the end of discharge represents the delivered charge relative to that obtained from a capacitor using pure RuO_2 electrodes.

The discharge curve for the capacitor employing M20B carbon has a lower slope and discharges to higher RAC than the curves for the capacitors employing FU1 and FU11B carbons. This suggests that M20B carbon is a better candidate material for use in electrochemical capacitors. The charge delivered by the M20B capacitor is more than 50% of the charge delivered if the electrodes were pure RuO_2, despite the fact that the electrodes in this capacitor are only 32% (by mass) RuO_2. Consideration of the structural parameters for these carbons (Table II) suggests an explanation. Although FU1 carbon produces an electrode with the lowest porosity and the highest faradaic surface area, M20B and FU11B carbons have larger internal surface areas and consequently, larger DL capacitances. The considerable DL capacitance of the carbon makes up for much of the lost faradaic pseudocapacitance in electrodes that are not pure RuO_2. Between the FU11B and M20B carbons, although the FU11B carbon has greater total specific surface area, the M20B carbon has more micropores and thus greater internal surface area ($\hat{S}_{C,int}$). Consequently, the M20B electrode has a much lower porosity as well as greater DL and faradaic surface areas (S_d and S_f) compared to FU11B. As expected, activated carbons with large internal surface areas are preferred because they increase the DL contribution to capacitance.

Table II. Properties of selected carbons ($x_C = 0.75$) with electrode characteristics calculated from packing theory (Appendix).

Carbon	FU1	FU11B	M20B
$\hat{S}_{C,int}$ (m^2/g) (Ref. 7)	517.6	1087	1245.5
$\hat{S}_{C,ext}$ (m^2/g) (Ref. 7)	23.4	510	98.1
d_C (nm)	142.5	6.56	33.9
$\gamma = d_{Ru}/d_C$	0.035	0.762	0.147
ε	0.173	0.367	0.205
S_f (cm^2/cm^3)	2.48×10^6	1.90×10^6	2.36×10^6
S_d (cm^2/cm^3)	8.52×10^6	15.53×10^6	16.82×10^6

Effect of carbon content.—The previous results show that electrodes containing mostly carbon can deliver a significant fraction of the charge that could be delivered by pure RuO_2 electrodes. Since activated carbon is much less expensive than RuO_2, it makes sense to explore the effect of carbon content on discharge performance. This, along with cost data, could be used to optimize the carbon content in composite electrodes. Figure 4 shows galvanostatic discharge curves for capacitor electrodes containing varying volume fractions of M20B carbon. M20B properties are shown in Table II, and parameters derived from packing theory calculations are given in Table III. As expected, the area under the discharge curve, proportional to total charge delivered, decreases as the volume fraction of carbon increases. Although the capacitance decreases with increasing carbon content, the RAC at the end of discharge remains relatively high. For example, when the electrodes contain 90% carbon by volume (only 13% RuO_2 by mass), the total delivered charge is still more than 30% of the theoretical maximum based on pure RuO_2.

Ragone plots provide a more comprehensive view of cell performance. We define energy and power densities as

$$\text{Energy density} = \frac{I_{cell}\Phi_{avg}t_d}{2L + L_s} \quad [41]$$

$$\text{Power density} = \frac{I_{cell}\Phi_{avg}}{2L + L_s} \quad [42]$$

where t_d is the total discharge time and Φ_{avg} is the average cell potential during discharge. Since the discharge curves (Fig. 4) are nearly linear in time and the cell potential decreases from 1.0 to 0 V, Φ_{avg} is assumed to be constant and equal to 0.5 V.

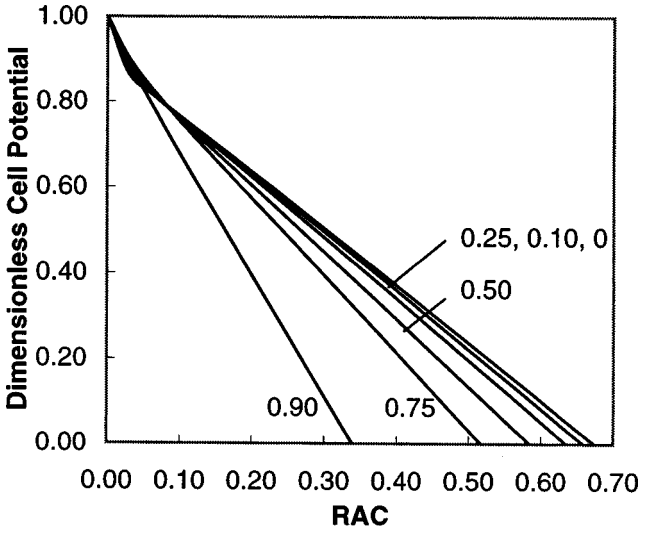

Figure 4. Galvanostatic discharge curves for capacitors with electrodes containing varying volume fractions of M20B carbon (values of carbon volume fraction shown on the lines). Parameters include $I_{cell} = 1.0$ A/cm^2, and $C_{s0} = 3.0$ M.

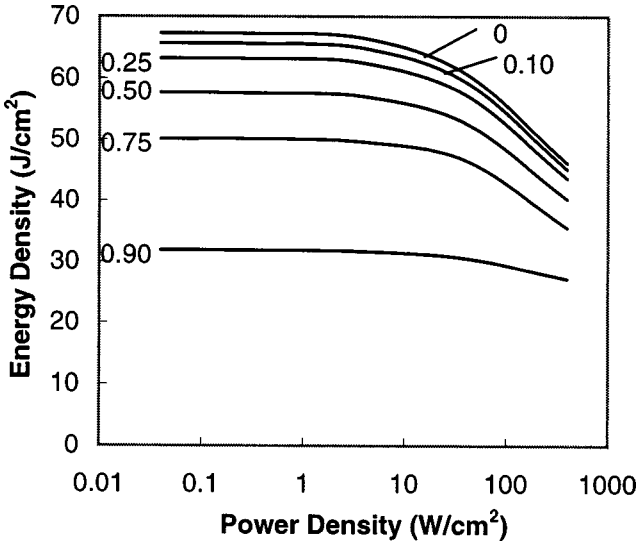

Figure 5. Ragone plot for capacitors with electrodes containing varying volume fractions of M20B carbon (values of carbon volume fraction shown on the lines). Parameters include $C_{s0} = 3.0$ M.

Figure 5 shows Ragone plots for capacitors with electrodes containing varying volume fractions of M20B carbon. This kind of plot can be used to establish the mass fractions of RuO_2 and carbon needed to achieve specified energy and power density requirements. As one might expect, energy density decreases with increasing carbon content and as power density increases. The power density is directly proportional to the cell current. The drop in energy density at high power density becomes less pronounced with increasing carbon content. The results suggest underutilization of the electrodes at high discharge rates. Results in the next section show that concentration polarization at high cell current density increases mass-transfer limitations for proton transport, leading to poorer discharge performance.

Current density and concentration polarization.—The results of Fig. 5 suggest a closer examination of performance as current density increases. Figure 6 presents galvanostatic discharge curves for capacitors with M20B carbon composite electrodes discharged at varying cell current densities. For discharge at relatively low current densities, the curves superimpose and are nearly linear. Such superposition is expected since RAC represents time made dimensionless using I_{cell} (Eq. 39). For discharge current densities greater than 0.1 A/cm^2, the curve shifts to the left, indicating less delivered charge (area under the curve) and lower electrode utilization (lower RAC at full discharge). With increasing discharge current density, both the DL and faradaic contributions to RAC decrease, although the impact is much greater on the faradaic pseudocapacitance (results not shown).

Examination of potential drop and electrolyte concentration profiles (Fig. 7 and 8) shows that concentration polarization within the electrode becomes significant as I_{cell} increases. With increasing I_{cell}, the potential drop in the electrolyte phase ($\overline{\Phi_2}$, Fig. 7) becomes non-negligible. As shown by Eq. 30, increasing $\overline{\Phi_2}$ leads to a lower overall cell potential at a given value of the "driving force" for discharge, E. This shifts the dimensionless discharge curves downward relative to their location in the absence of concentration polarization. Significant concentration gradients (Fig. 8) that develop in the electrolyte phase suggest that mass-transfer limitations are detrimental to capacitor performance at high discharge rates.

Optimum porosity.—As discussed earlier, the carbon pore size distribution, quantified here by the internal and external specific surface areas ($\hat{S}_{C,int}$ and $\hat{S}_{C,ext}$, representing micropore and meso/macropores, respectively), has an important influence on electrode porosity and thus performance. Equation 4 shows that decreasing $\hat{S}_{C,ext}$ increases the carbon equivalent diameter and thus decreases porosity (see Appendix). In effect, decreasing the diameter ratio

Table III. Electrode characteristics calculated from packing theory (Appendix) for various volume fractions of M20B carbon.

x_C	ε	S_f (cm^2/cm^3)	S_d (cm^2/cm^3)
0	0.375	7.50×10^6	7.50×10^6
0.10	0.357	6.94×10^6	8.50×10^6
0.25	0.327	6.06×10^6	10.13×10^6
0.50	0.271	4.37×10^6	13.19×10^6
0.75	0.205	2.39×10^6	16.82×10^6
0.90	0.316	0.821×10^6	15.71×10^6

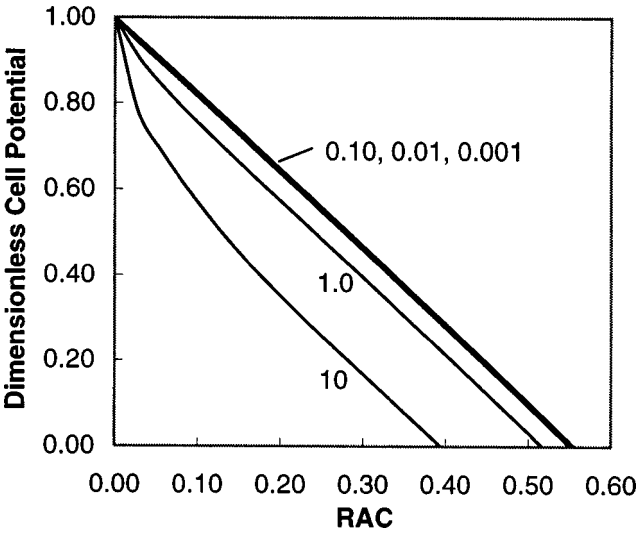

Figure 6. Galvanostatic discharge curves for capacitors discharged at varying cell current densities (values of discharging current density, in A/cm^2, shown on the lines). Parameters include $I_{cell} = 1.0$ A/cm^2, $C_{s0} = 3.0$ M, and $x_C = 0.75$ (M20B carbon).

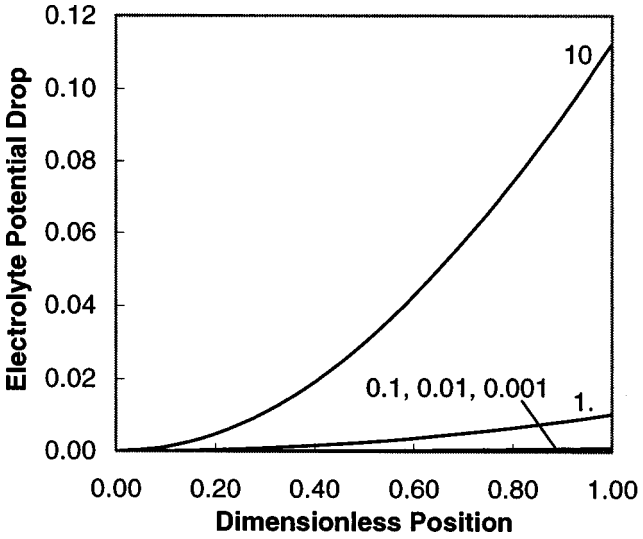

Figure 7. Potential distribution in the electrolyte phase near the end of galvanostatic discharge of capacitors discharged at varying cell current densities (values of discharging current density, in A/cm^2, shown on the lines). Parameters as in Fig. 6.

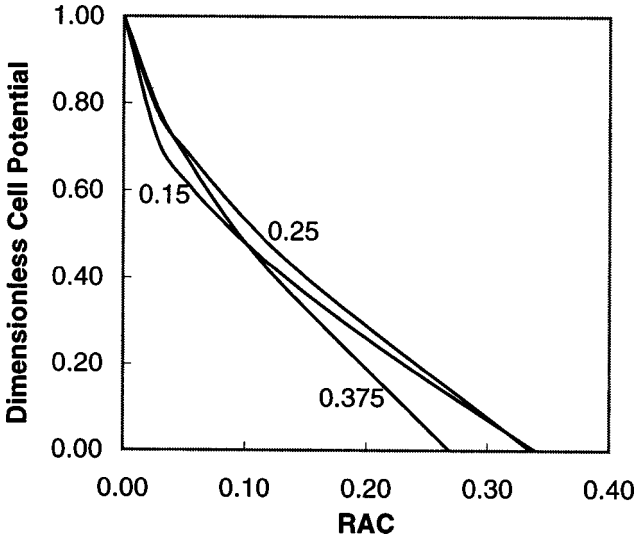

Figure 9. Galvanostatic discharge curves for capacitors having varying porosities but constant carbon specific surface area (values of porosity shown on the lines). Parameters include $\rho_C(\hat{S}_{C,int} + \hat{S}_{C,ext}) = 20 \times 10^6$ cm^2/cm^3, $I_{cell} = 1.0$ A/cm^2, $C_{s0} = 3.0$ M, and $x_C = 0.75$ (M20B carbon).

makes it possible to achieve a higher packing fraction through more efficient packing of small particles into the voids between larger particles (see Fig. 3 of Ref. 14). As porosity decreases, the DL and faradaic surface areas per unit volume of electrode both increase (Eq. 5 and 6). This should increase the total delivered charge (*i.e.*, the area under the discharge curve). Equation 35 shows that decreasing porosity sharply reduces the effective ionic conductivity of the electrolyte in the porous electrode. Ultimately, concentration polarization should become important and limit performance. Thus an optimum porosity may exist.

We investigate this hypothesis by studying a hypothetical carbon with constant total surface area, $\rho_C(\hat{S}_{C,int} + \hat{S}_{C,ext})$, but varying amounts of internal and external surface area, $\hat{S}_{C,int}$ and $\hat{S}_{C,ext}$. Varying the latter changes the porosity. The sum $\rho_C(\hat{S}_{C,int} + \hat{S}_{C,ext})$ remains constant in Eq. 5, so the DL and faradaic specific areas only change with ε. Figure 9 shows discharge curves for selected porosities. Upon decreasing the porosity from 0.375 to 0.25, the discharge curve moves up, implying increases in the total delivered charge and electrode utilization (relative to pure RuO_2). However, further decrease in porosity (to 0.15) impacts the performance of the system due to the effects of concentration polarization. Thus, discharge performance depends not only on the total specific surface area, but also on the distribution of that surface area as represented by porosity. Further quantification should lead to identification of the optimal porosity that maximizes discharge current density as a function of cell voltage and other design parameters.

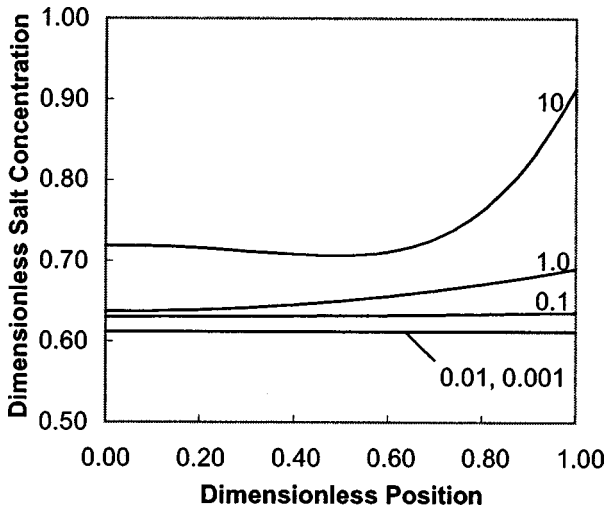

Figure 8. Salt concentration distribution in the electrolyte phase near the end of galvanostatic discharge of capacitors at varying cell current densities (values of discharging current density, in A/cm^2, shown on the lines). Parameters as in Fig. 6.

Conclusion

The effects of composition variations, particle packing, and concentration polarization have been incorporated in an extension of the previous model by Lin *et al.*[13] We have used this model to investigate the effects of varying carbon type, carbon mass/volume fraction, and discharge current density on the performance of RuO_2/C electrochemical capacitors. Under all conditions, polarization of the electrolyte has a significant effect on discharge performance and must be incorporated in realistic models of electrochemical capacitor charge/discharge. Among the many available activated carbons,[7] ones with relatively large internal surface areas (micropores) but low external surface areas should be most useful for maximizing both DL capacitance and faradaic pseudocapacitance. These characteristics increase the specific surface area for DLs as well as favor better packing of RuO_2 within the carbon. At high discharge current densities, one may use electrodes containing substantial amounts of carbon without greatly sacrificing performance, particularly energy density (Fig. 5). Because the carbon provides significant DL capacitance but costs much less than RuO_2, one should be able to find an optimum composition that provides acceptable performance and minimum cost under specified discharge conditions.

Acknowledgments

We acknowledge the financial support of this work by the South Carolina Commission on Higher Education and the U.S. Army Research Office under grant no. DAAH04-96-1-0422.

The University of South Carolina assisted in meeting the publication costs of this article.

Appendix
Packing Theory Calculation of Porosity

The composition of the electrode may be expressed in terms of the mass fractions f_i (i = C, RuO_2) or volume fractions based on solid volume given by

$$x_i = \frac{f_i/\rho_i}{\Sigma_j f_j/\rho_j} \quad [A\text{-}1]$$

in which the sum runs over the two solid components. The porosity ε may be calculated in terms of the particle size ratio $\gamma = d_R/d_C$ and the component volume fractions using the packing theory developed by Yu *et al.*[22] Starting with a matrix of large particles (carbon), filling the voids with small particles (RuO_2) produces a composite with specific volume V_L given by

$$V_L = Vx_c + \hat{V}_S x_{Ru} \quad [A\text{-}2]$$

where $V = 1.6$ is the specific volume for random packed spheres and $\hat{V}_S$ is the partial specific volume of the small particles, given by

$$\hat{V}_S = V[1 - (1 - \gamma)^{3.3} - 2.8\gamma(1 - \gamma)^{2.7}] \quad [A\text{-}3]$$

Alternately, starting with a matrix of small particles and replacing portions of the matrix with large particles, the specific volume V_S is

$$V_S = Vx_{Ru} + \hat{V}_L x_{ac} \quad [A\text{-}4]$$

Here $\hat{V}_L$ is the partial specific volume of the large particles, calculated as

$$\hat{V}_L = V - (V - 1)[(1 - \gamma)^{2.0} + 0.4\gamma(1 - \gamma)^{3.7}] \quad [A\text{-}5]$$

The specific volume of the mixture, V_m, and electrode porosity, ε, are given by

$$V_m = \max\{V_S, V_L\} \quad [A\text{-}6]$$

and

$$\varepsilon = 1 - 1/V_m \quad [A\text{-}7]$$

List of Symbols

C dimensionless electrolyte concentration
C_d double-layer capacitance per area of electrode, F/cm^2
C_0 solvent concentration, mol/cm^3
C_s electrolyte concentration, mol/cm^3
C_{s0} initial electrolyte salt concentration, mol/cm^3
C_{total} total available charge per electrode area in pure RuO_2 electrode, C/cm^2
D_i diffusion coefficient (i = +,−,s), cm^2/s
D_{i0} diffusion coefficient for cations, anions, and electrolyte salt in the bulk solution (i=+,−,s), cm^2/s
$D_{s,s}$ salt diffusion coefficient in the separator, cm^2/s
d_C effective carbon particle diameter, cm
d_{Ru} RuO_2 particle diameter, cm
E local potential difference between matrix phase and electrolyte phase, V
E_0 initial local potential difference between matrix and electrolyte phases ($\equiv 2V_0$), V
$f_\pm$ electrolyte activity coefficient
f_C carbon mass fraction in composite electrode
f_{Ru} RuO_2 mass fraction in composite electrode
h edge length of crystal lattice unit cell for RuO_2, cm
i_0 exchange current density for the electrode reaction, A/cm^2
i_1 superficial current density in the matrix phase, A/cm^2
i_2 superficial current density in the electrolyte phase, A/cm^2
I_{cell} cell discharge current density, A/cm^2
j_f faradaic transfer current density for the RuO_2 redox reaction, A/cm^2
J dimensionless faradaic transfer current density for the RuO_2 redox reaction
L thickness of the electrode, cm
L_s length of the separator, cm
L_A Avogadro's number, 6.0226×10^{23}/mol
n number of electrons transferred in electrode reaction
$Q_{f,ox}$ faradaic charge per unit volume of the fully oxidized electrode, C/cm^3
$Q_{f,red}$ faradaic charge per unit volume of the fully reduced electrode, C/cm^3
RAC relative available charge
s_+ stoichiometric coefficient of cations in electrode reaction
S_d specific surface area for double-layer capacitance per unit electrode volume, cm^2/cm^3
S_f specific surface area for faradaic capacitance per unit electrode volume, cm^2/cm^3
$\hat{S}_{C,int}$ internal specific surface area of carbon, cm^2/g
$\hat{S}_{C,ext}$ external specific surface area of carbon, cm^2/g
T temperature, K
t time, s
t_0 time constant for double layer, s
t_+^0 cation transference number
t_d total discharge time, s
U dimensionless equilibrium potential for electrode reaction (*vs.* SCE)
U_1 equilibrium potential for electrode reaction (*vs.* SCE), V
V specific volume for random packed spheres
V_L specific volume defined in Eq. A-2
V_S specific volume defined in Eq. A-4
$\hat{V}_L$ partial specific volume defined in Eq. A-5
$\hat{V}_S$ partial specific volume defined in Eq. A-3
V_m specific volume of a mixture of large and small particles
V_0 initial equilibrium potential before charging (*vs.* SCE), V
x position across the cell, cm
X dimensionless position across the cell
x_C carbon volume fraction in the composite electrode
x_{Ru} RuO_2 volume fraction in the composite electrode
z_i charge number of cations and anions (i = +, −)

Greek

α_a anodic transfer coefficient of the electrode reaction
α_c cathodic transfer coefficient of the electrode reaction
γ RuO_2/carbon particle diameter ratio
ε electrode porosity
ε_s separator porosity
E dimensionless local potential difference between matrix phase and electrolyte phase
θ local molar fraction of oxidized RuO_2
κ_p ionic conductivity of electrolyte within the porous electrode, S/cm
κ_{p0} ionic conductivity of electrolyte in bulk solution, S/cm
ν_+ number of cations into which a mole of electrolyte salt dissociates
ρ_C carbon density, g/cm^3
ρ_{Ru} RuO_2 density, g/cm^3
σ electronic conductivity in the matrix phase, S/cm
τ dimensionless time
Φ_1 potential in the matrix phase, V
$\overline{\Phi}_1$ dimensionless potential in the matrix phase
Φ_2 potential in the electrolyte phase, V
$\overline{\Phi}_2$ dimensionless potential in the electrolyte phase
$\overline{\Phi}_{cell}$ dimensionless cell potential drop
Φ_{avg} average cell potential during discharge, V

References

1. C. Lin, J. A. Ritter, and B. N. Popov, *J. Electrochem. Soc.*, **146**, 3155 (1999).
2. J. P. Zheng, *Electrochem. Solid-State Lett.*, **2**, 359 (1999).
3. J. M. Miller, B. Dunn, T. D. Tran, and R. W. Pekala, *J. Electrochem. Soc.*, **144**, L309 (1997).
4. B. E. Conway, *J. Electrochem. Soc.*, **138**, 1539 (1991).
5. B. E. Conway, V. Birss, and J. Wojtowicz, *J. Power Sources*, **66**, 1 (1997).
6. B. E. Conway, *Electrochemical Supercapacitors: Scientific Fundamentals and Technological Applications*, Kluwer Academic/Plenum, New York (1999).
7. H. Shi, *Electrochim. Acta*, **41**, 1633 (1996).
8. J. P. Zheng, P. J. Cygan, and T. R. Jow, *J. Electrochem. Soc.*, **142**, 2699 (1995).
9. T. R. Jow and J. P. Zhang, *J. Electrochem. Soc.*, **145**, 49 (1998).
10. A. M. Johnson and J. Newman, *J. Electrochem. Soc.*, **118**, 405 (1971).
11. D. Dunn and J. Newman, *J. Electrochem. Soc.*, **147**, 820 (2000).
12. V. Srinivasan and J. W. Weidner, *J. Electrochem. Soc.*, **146**, 1650 (1999).
13. C. Lin, J. A. Ritter, B. N. Popov, and R. E. White, *J. Electrochem. Soc.*, **146**, 3168 (1999).
14. G. S. Nagarajan, J. W. Van Zee, and R. M. Spotnitz, *J. Electrochem. Soc.*, **145**, 771 (1998).
15. R. Darling and J. Newman, *J. Electrochem. Soc.*, **144**, 4201 (1997).
16. J. M. Heikonen, H. J. Ploehn, and R. E. White, *J. Electrochem. Soc.*, **145**, 1840 (1998).
17. J. C. Card, G. Valentin, and A. Storck, *J. Electrochem. Soc.*, **137**, 2736 (1990).
18. J. Newman, *Electrochemical Systems*, 2nd ed., Prentice-Hall, Englewood Cliffs, NJ (1991).

19. J. Newman and W. Tiedemann, *AIChE J.*, **21**, 25 (1975).
20. B. Leimkuhler, L. R. Petzold, and C. W. Gear, *SIAM (Soc. Ind. Appl. Math.) J. Numer. Anal.*, **28**, 205 (1991).
21. M. Doyle, T. F. Fuller, and J. Newman, *J. Electrochem. Soc.*, **140**, 1526 (1993).
22. A. B. Yu, R. P. Zou, and N. Standish, *Ind. Eng. Chem. Res.*, **35**, 3730 (1996).
23. S. Trasalti and G. Lodi, in *Electrodes of Conductive Metallic Oxides, Part A*, S. Transalti, Editor, p. 301, Elsevier, New York (1980).
24. P. Pillay and J. Newman, *J. Electrochem. Soc.*, **143**, 1806 (1996).